Enhancer heterogeneity of lung neuroendocrine tumors reveals sensitivity to FGF signaling inhibition

Ester Davis[1,*], Shani Avniel-Polak[2,*], Shahd Abu-Kamel[1], Israel Antman[1], Tsipora Saadoun[1], Chava Brim[1], Anat Bel-Ange[2], Karine Atlan[3,4], Tomer Tzur[4,5], Firas Abu Akar[6], Ori Wald[4,7], Uzi Izhar[4,7], Merav Hecht[1], Simona Grozinsky-Glasberg[2,4], Yotam Drier[1]

[1] The Lautenberg Center for Immunology and Cancer Research, IMRIC, Faculty of Medicine, Hebrew University of Jerusalem, Israel

[2] The Neuroendocrine Tumor Unit, ENETS Center of Excellence, Hadassah Medical Center, Jerusalem, Israel.

[3] Department of Pathology, Hadassah Medical Center, Jerusalem, Israel

[4] Faculty of Medicine, Hebrew University of Jerusalem, Israel

[5] Department of Plastic and Reconstructive Surgery, Hadassah Medical Center, Jerusalem, Israel

[6] Department of Thoracic Surgery, The Edith Wolfson Medical Center, Holon, Israel Affiliated to the Sackler Faculty of Medicine, Tel Aviv University, Tel Aviv, Israel.

[7] Department of Cardiothoracic Surgery, Hadassah Medical Center, Jerusalem, Israel

* These authors contributed equally: Ester Davis, Shani Avniel-Polak

Corresponding authors: simonag@hadassah.org.il (SGG) and yotam.drier@mail.huji.ac.il (YD).

Well differentiated low grade lung neuroendocrine tumors (lung carcinoids or LNETs) are histo-pathologically classified as typical and atypical LNETs, but each subtype is still heterogenous both at the molecular level and its clinical manifestation. Therefore, the treatment of patients with LNETs is challenging. The two main challenges are the lack of effective drug treatments and the lack of reliable biomarkers to guide management since the disease in patients with the same tumor grade/stage often have different clinical courses. The genetic, epigenetic, and developmental programs that drive LNETs remain obscure, limiting our abilities to suggest new biomarkers and drug targets. Here we report for the first time genome-wide profiles of cis-regulatory elements. Analysis of these regulatory landscapes uncovered three regulatory subtypes even within typical LNETs. Comparing enhancer acetylation across subtypes revealed different differentiation signals, one driven by ASCL1, SOX4 and BARX1 factors invoking neuronal-like signature and one driven by HNF1 and HNF4 factors. The HNF+ subtype demonstrated strong enhancers near FGF signaling genes, and differential expression of FGF pathway genes, especially FGFR3. Indeed in-vitro

and in-vivo FGF inhibition delays HNF+ LNETs growth, suggesting new therapeutic strategies.

Functioning cis-regulatory elements known as enhancers bind transcription factors (TFs) and the flanking histones bear chemical modifications such as H3K27ac[1]. Enhancer profiling of tumor samples can reveal useful biological and clinical insights into tumor ontogeny[2–4]. ChIP-seq-derived profiles of H3K27ac marked candidate enhancers in 16 primary typical and 2 atypical lung neuroendocrine tumors (Suppl. Table 1) demonstrate remarkable heterogeneity (Fig. 1a, Supp. Fig. 1), similar in scale to heterogeneity between different types of neuroendocrine tumors (Fig. 1b).

Clustering of cis-regulatory landscapes reveals three potential regulatory subtypes. Pathway analysis of differential enhancers suggests one subtype (henceforth neural-like LNET) is enriched with genes related to neuronal differentiation, as suggested by the enrichment of the 'Neuron' and 'Synapse' GO terms (Table 1, Suppl. Table 2). These tumors exhibit strongly acetylated enhancers near related genes such as ASCL1, SOX4, BARX1, SMPD3, PHACTR3, and ETV1 (Fig. 1c). Indeed, neural-like specific enhancers were enriched with the binding motif of ASCL1, SOX4, ETV1 and BARX1 transcription factors, suggesting they bind enhancers and regulate transcription in neural-like NETs (Fig. 1d, Suppl. Table 3).

MSigDB Term	p-value	Relative Enrichment
GO_SYNAPSE	1.43E-07	1.89
GO_NEURON_PART	1.54E-07	1.66
GO_SYNAPSE_PART	2.9E-07	1.99
KONDO_PROSTATE_CANCER_WITH_H3K27ME3	3.24E-07	3.66
GO_CELL_JUNCTION	1.21E-06	1.64

Table 1: Top five MSigDB terms enriched in genes near enhancers significantly more acetylated (fold-change > 2, FDR < 10%) in neural-like LNETs compared to HNF+ LNETs.

Another prominent subtype (henceforth HNF+ LNET) exhibit enhancers near HNF targets, as indicated by enrichment of HNF1A targets and liver specific genes (Table 2, Suppl. Table 2). Indeed, these tumors exhibit strongly acetylated enhancers near related genes such as HNF1A, HNF4A, CEACAM1, PPARGC1A, FOXA3, RXRA, FBXW7, HGD and HPN (Fig. 1c). Motif analysis of HNF+ LNETs enhancers reveled strong enrichment of the HNF1, HNF4, PPAR and RXR motifs (Fig. 1e, Suppl. Table 3). Binding sites of HNF1A and HNF4A (In HepG2 cells, data from ENCODE, see methods) are found in 54.2% (1137 / 2099) HNF+ LNET enhancers, compared to only 12.4% (287 / 2314) of neural-like enhancers, suggesting much of the differences in enhancer landscape is due to activation of HNF1A and HNF4A. Of note, the H3K27ac peak at the HNF1A locus spans the promoters of both HNF1A and a

lncRNA known as HNF1A-AS1, transcribed from the other strand. Both genes are expressed specifically in HNF+ LNETs, and HNF1A-AS1 to an even greater extent (Supp. Fig. 2).

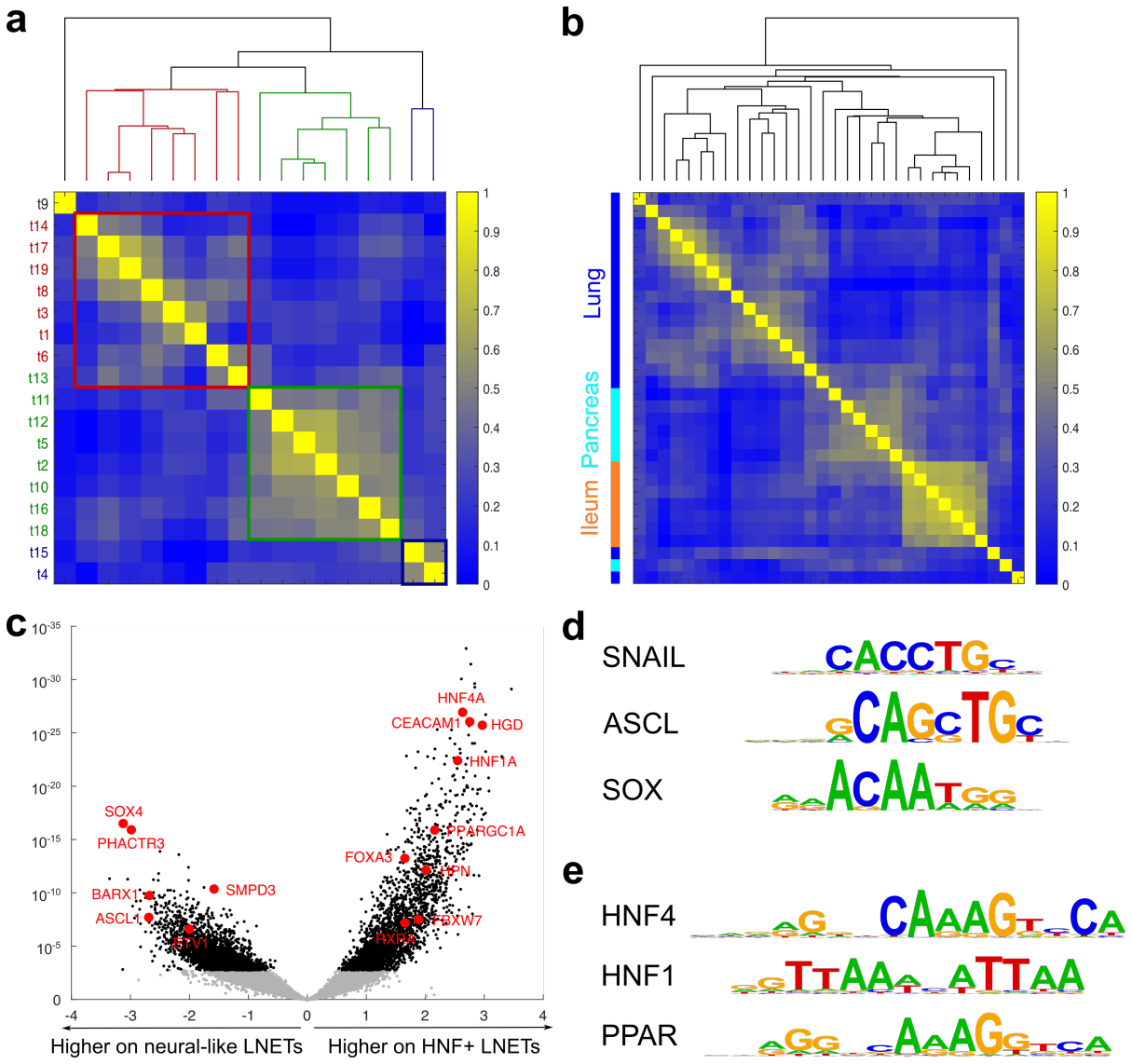

Figure 1: (a) Pairwise Spearman correlations of H3K27ac signals at distal regulatory elements in lung neruroendocrine tumors suggest three possible regulatory subtypes. Tumors in the first cluster (termed Neural-like LNETs) are marked in red, second cluster (termed HNF+ LNETs) marked in green, and the third in blue. **(b)** Pairwise Spearman correlations of H3K27ac signals across lung, pancreatic and ileal neuroendocrine tumors demonstrate high dissimilarity between lung NETs subtypes, with similar magnitude as between different types of neuroendocrine tumors. **(c)** Significance ($\log_{10}$ scale, Wald's test) and log2 fold differences in H3K27ac ChIP-seq signals in HNF+ and neural-like LNETs, calculated by DESeq2 comparison of 15 biologically independent tumors. Each dot represents an individual site (black: FDR < 0.01). Selected H3K27ac sites are marked by red circle and annotated by the nearest gene. **(d-e)** Top three motif families enriched in neural-like LNETs **(d)** and HNF+ LNETs **(e)** specific enhancers.

The third subtype does not show any clear differentiation signals or master transcription factors, possibly due to the small number of samples in our cohort. It displays unique strong enhancers near several genes such as CCKBR, PARVB and B3GALNT1. It also displays acetylation in many of the HNF+ LNETs enhancers, including at HNF1A, HNF4A, CEACAM1,

FOXA3 and HGD. However, SOX4 enhancers, one of the key markers of neural-like LNETs are also acetylated. This agrees with previous integrative analyses[5,6] that identified three molecular LNET subtypes.

MSigDB Term	p-value	Relative Enrichment
SERVITJA_ISLET_HNF1A_TARGETS_DN	9.19E-14	4.82
MEISSNER_BRAIN_HCP_WITH_H3K4ME3_AND_H3K27ME3	1.98E-11	1.88
HSIAO_LIVER_SPECIFIC_GENES	2.66E-09	2.91
LI_WILMS_TUMOR_VS_FETAL_KIDNEY_1_UP	3.59E-08	2.84
CHYLA_CBFA2T3_TARGETS_DN	6.77E-08	2.67

Table 2: Top five MSigDB terms enriched in genes near enhancers significantly more acetylated (fold-change > 2, FDR < 10%) in HNF+ LNETs compared to neural-like LNETs.

Next, we focused on super-enhancers. Across all tumors 2021 super-enhancers were identified. Of those 590 overlapped with the neural-like enriched enhancers, 474 with HNF+ enriched enhancers, and another 379 enriched in the third subtype, demonstrating most super-enhancers are differential between the subtypes. Many of the enhancers mentioned above are in fact super-enhancers, such as INSM1, SOX4, PHACTR3, HNF1A, HNF4A and FOXA3. The top 10 differential super enhancers are near C2orf72, BCL2L10, RUVBL1, HNF4A, HGD, FGFR3, TTBK1, TM4SF5, SLC12A8 and MUCL1, all more strongly acetylated in HNF+ LNETs. Since FGFR3 is important for tumor growth and can be targeted by small molecule drugs we further focused on FGF signaling in HNF+ LNETs.

We have therefore tested FGF inhibition by treating three lung neuroendocrine neoplasms cell lines (two of human well-differentiated LNET origin, NCI-H727 and NCI-H835), and one of a human lung neuroendocrine carcinoma origin, NCI-H1770, respectively) with either Erdafitinib or Lenvatinib, for 24, 48 and 72 hours, and tested their impact of cell viability. Lenvatinib is a multitargeting tyrosine kinase inhibitor which targets the VEGFR and FGFR receptors and has been reported to be effective in advanced pancreatic and gastrointestinal NETs[7]. Erdafitinib is a pan-FGFR tyrosine kinase inhibitor with minimal activity on VEGFR kinases. Out of the three, only NCI-H727 showed sensitivity to Lenvatinib and Erdafitinib (Fig. 2a), with less than 50% viable cells at 15μM suggesting this is the only cell line relying on FGF signaling. NCI-H835 on the other hand demonstrated remarkable resistance to both Lenvatinib and Erdafitinib. We profiled enhancers by H3K27ac ChIP-seq in these cell lines, and as expected, only NCI-H727 has an active enhancer at the FGFR3 locus (Fig. 2b). The global enhancer landscape of the cell lines is considerably different than that of primary LNETs (Supp. Fig. 3), probably due to inherent limitations of in-vitro cell line models, such as different environmental factors, in-vitro selection pressures, and genetic drift and instability. However, NCI-H727 do retain the main HNF+ marker enhancers near HNF1A, HNF4A, CEACAM1,

FOXA3, HGD and HPN (Supp. Fig. 2,4). NCI-H835, the most resistant line to FGF inhibition display acetylation at the key neural-like enhancers ASCL1, BARX1, SMPD3 and SOX4 (Supp. Fig. 5).

Since NCI-H835 is not sensitive to FGFR inhibition, but still display strong acetylation at many neural-like NET super-enhancers, we next tested if it may be sensitive to inhibition of super-enhancer activity by the novel small molecule multi-kinase inhibitor A51[8]. All three cell lines show similar sensitivity to A51 (Fig. 2c), suggesting super-enhancer targeting drugs may be helpful across lung neuroendocrine subtypes. On the molecular level the effect of A51 was cell line specific, where genes downregulated by A51 were enriched in the Neuron Development and Synapse GO terms in NCI-H835 cells and in liver specific genes in NCI-H727 cells (Suppl. Table 2). This suggests that super-enhancers drive the neural-like and HNF+ patterns of NCI-H835 and NCI-H727, respectively, and that A51 can target this identity by perturbing super-enhancer function. Interestingly, liver-specific genes were upregulated by A51 in NCI-H835 suggesting perhaps that once neural identity is lost HNF+ differentiation is activated.

Erdafitinib demonstrated a high efficacy in NCI-H727 cells and may therefore be a promising new direction to treat HNF+ LNETs. To further test this hypothesis in-vivo, we generated a mouse xenograft LNET model by subcutaneous injection of NCI-H727 cells to the back of the athymic nude mouse. H3K27ac profiles of tumors obtained from this mouse model are very similar to NCI-H727 cells grown in-vitro (Supp. Fig. 3), suggesting the differences observed between cell lines and primary tumors is not due to differences in the microenvironment or environmental factors, and cannot be easily reverted. Importantly, treating these mice daily with Erdafitinib (12.5mg/kg) significantly slows down tumor growth in-vivo (Fig. 2d). Repeating this experiment yielded similar results (Supp. Fig. 6A,B), demonstrating its robustness. Treating with Lenvatinib (5mg/kg) may also slow down tumor growth, even if to somewhat lesser extent (Supp. Fig. 6B,C).

In conclusion this study demonstrates the utility of enhancer profiling and provides an important resource to better understand and treat lung neuroendocrine tumors. Several findings have clear clinical significance, and can serve as a basis for future clinical studies: 1) LNET patients may benefit from super-enhancer targeting drugs such as A51; 2) Patients with HNF+ LNET may benefit from FGFR inhibition-based treatment; 3) Specific FGFR inhibitors such as Erdafitinib may be a better fit than broader kinase inhibitors such as Lenvatinib; 4) Kinase inhibitors may work better on patients with HNF+ LNET than on patients with other subtypes of LNETs, and they could be identified by measuring FGFR3 or HNF4A.

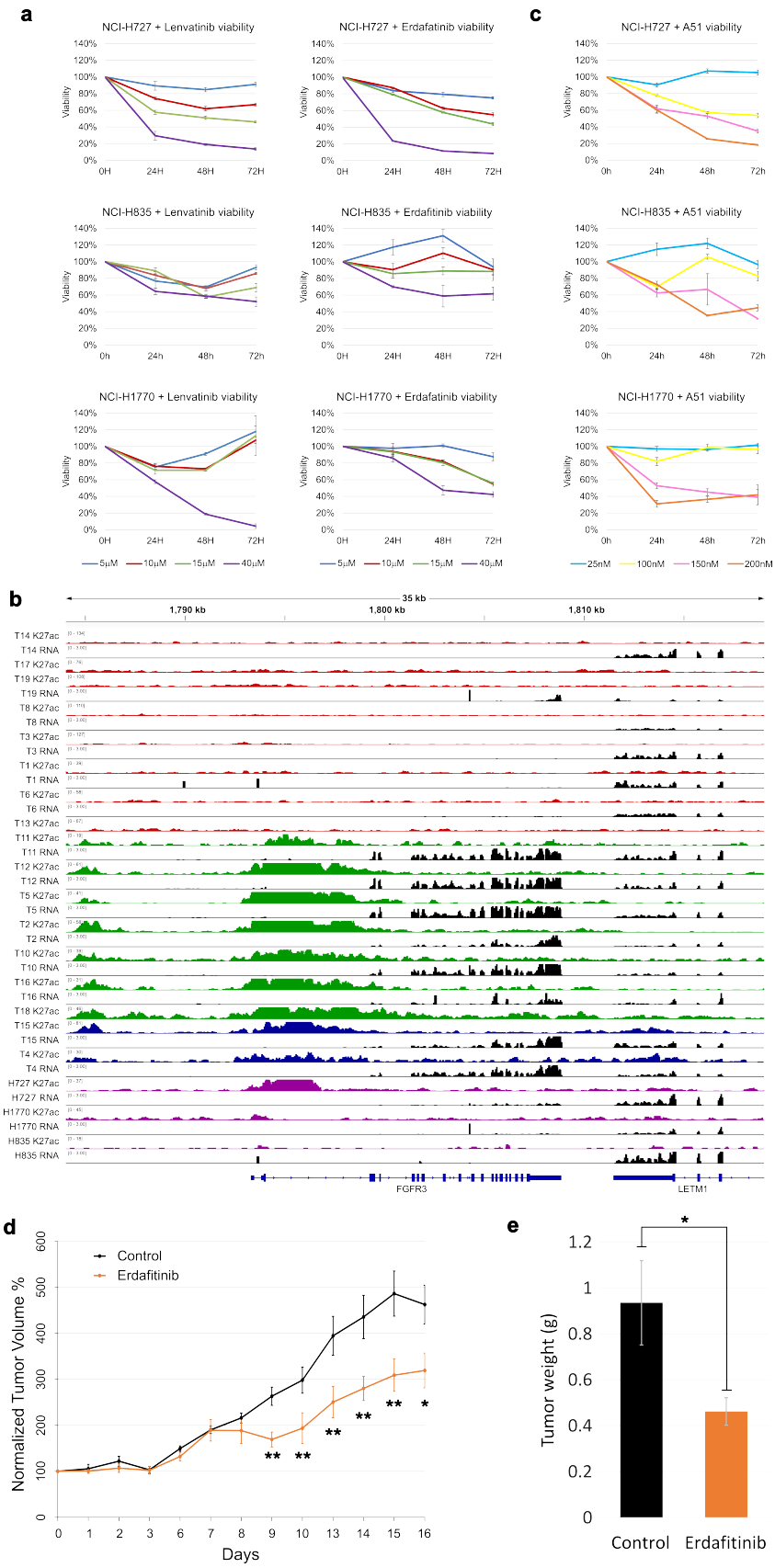

Figure 2: (a) Relative cell line viability as measured by WST-1 assay of the NCI-H727, NCI-H835 and NCI-H1770 during treatment with Lenvatinib (left) or Erdafitinib (right). Values represent ratio between viability of treated cells and of control cells treated with DMSO. Error bars represent standard error of the mean. **(b)** Genomic view of the FGFR3 locus, showing RNA signal (black) and H3K27ac signals of neural-like (red), HNF+ (green) and third cluster (blue) lung neuroendocrine tumors, as well as the NCI-H727, NCI-H1770 and NCI-H835 lung neuroendocrine neoplasms cell lines (purple). RNA-seq signals are normalized to 3 bins per million mapped reads (BPM). H3K27ac signals are scaled by promoter-based DESeq2 normalization (see Methods). **(c)** Relative cell line viability as measured by WST-1 assay of the NCI-H727, NCI-H835 and NCI-H1770 during treatment with A51. Values represent ratio between viability of treated cells and of control cells treated with DMSO. Error bars represent standard error of the mean. **(d)** Normalized tumor volume of NCI-H727 mouse xenograft model treated with Erdafitinib (12.5mg/kg, orange) or PBS 1% tween control (black). Error bars represent standard error of the mean. P-values are calculated by one tail t-test, * $p < 0.05$, ** $p < 0.01$. **(e)** Average tumor weight of the PBS control group (black) and Erdafitinib treated group (orange) at the end of the experiment after mice were sacrificed. Error bars represent standard error of the mean. P-values are calculated by one tail t-test, * $p < 0.05$.

Methods

Clinical materials: Fresh-frozen LNET specimens were obtained from patients treated at the Neuroendocrine Tumor Unit, ENETS Center of Excellence, Hadassah Medical Center, Jerusalem, Israel, under the Hadassah Institutional Helsinki committee, approval no. 0627-20-HMO.

RNA-seq: 2mm tissue sample was homogenized in tri-reagent and RNA was extracted flowing the standard tri-reagent protocol. After precipitation RNA was resuspended in appropriate volume of Rnase free water supplemented with RNA inhibitors (New England Biolabs). RNA samples were stored at -80°C until further use. The quality of the extracted RNA was assessed using the Agilent TapeStation System. 250 ng RNA was used to generate RNA-seq libraries using the KAPA mRNA Hyperprep Kit according to the manufacturer's instructions. Sequence data have been deposited at the European Genome-phenome Archive (EGA), which is hosted by the EBI and the CRG, under accession number EGAS50000000058.

Chromatin immunoprecipitation sequencing (Chip-seq): Chip-seq was performed as previously described[9]. In brief, cultured cells or minced frozen tissue were crosslinked in 1% formaldehyde. Sonication of samples were calibrated such that DNA was sheared to 300-700bp fragments. Histone H3K27 acetylation was immunoprecipitated using antibody from Active Motif (no. 39133). ChIP DNA was used to generate sequencing libraries using KAPA Hyper Prep Kit. Sequence data have been deposited at the European Genome-phenome Archive (EGA), which is hosted by the EBI and the CRG, under accession number EGAS50000000057.

Cell lines and inhibitors experiments: Lenvatinib and Erdafitinib (JNJ-42756493) were purchased from MedChemExpress (NJ, USA). The A51 inhibitor was a kind gift from Prof. Yinon Ben-Neriah. NCI-H727, NCI-H1770 and NCI-H835 cell lines were acquired from ATCC. The cell lines were cultured in complete RPMI 1640 media (Gibco, Thermo Fisher Scientific, Massachusetts, USA) supplemented with 10% or 5% fetal bovine serum (FBS; HyClone, Utah, UK), 1% penicillin streptomycin (Diagnovum, Tilburg, Netherlands), 1% L-glutamine (Sartorius, Göttingen, Germany), 1% sodium pyruvate (Sartorius), and 1% non-essential amino acids (Diagnovum). The WST-1 cell viability assay (Abcam, Cambridge, England) was performed on the three cell lines by seeding cells in 100µl into individual wells of a 96-well plate. The cells were treated with different concentrations of inhibitors or DMSO control for 24h, 48h and 72h. After the respective incubation periods, 10µl WST-1 reagent was added to each well and incubated for 2-4 h. The plates were then scanned

using a microplate spectrophotometer (Multiskan GO, Thermo Scientific, Massachusetts, USA) at wavelengths of 450 nm and 650 nm. The resulting data were analyzed to assess cell viability at each concentration and time point.

In-vivo inhibitor experiments. LNET xenografts were established 5 days following the subcutaneous injection of $4*10^6$ NCI-H727 cells to the back of athymic nude mouse (FOXN1NU NU/NU mouse). Once the neoplasm size reached $130mm^3$, the mice were randomized into 2 groups and treated for the next 4 weeks with: (1) vehicle1% Tween 80 (2) Erdafitinib (JNJ-42756493) 12.5mg/kg dissolved in 1% Tween 80, (N=7) Animals were treated daily (except for weekends) for 20 days; drugs were administered by oral gavage. Tumor size was measured daily using a caliper, and its volume was estimated using the equation: length * $(width^2)/2$. Drug concentrations were chosen after conducting calibration experiments with the recommended concentrations. Experiment repetition was performed using the same model with minor changes. Mice were randomized into 3 groups and treated for the next 4 weeks with: (1) vehicle 0.5% carboxymethylcellulose (CMC), (2) Lenvatinib (5mg/kg) dissolved in 0.5% CMC, (3) Erdafitinib (JNJ-42756493) 12.5mg/kg dissolved in 1% Tween 80. Animals were treated daily (N=6), and the tumor volume was calculated as described before.

Computational and statistical analyses. ChIP-seq reads were aligned to the reference genome (hg38) using BWA 0.7.17 (Ref. [10]). Reads with mapping quality < 10 were not counted, and reads aligned to the same position and strand were only counted once. Density signals were calculated by deeptools's bamCoverage[11] and visualized on the Integrated Genome Viewer[44]. Regular H3K27ac peaks were called using HOMER[12], with style 'histone' for variable length, and super-enhancer using style 'super' and requiring local fold change of 1 (-L 1). We generated a union set of H3K27ac peaks by taking the top 40,000 peaks of each sample, removing ENCODE blacklisted peaks, and merging all remaining peaks using bedtools merge[13]. Acetylation signal was estimated from ChIP-seq reads that fell within this union set of H3K27ac peaks. To compare and acetylation at peaks between peaks, we used DESeq2 (Ref. [14]) for read counts computed with featureCounts[15]. Promoter signals (<2 kb downstream and <2.5 kb upstream of TSSs) vary less than those at enhancers and were therefore used to calculate normalization factors (size factor, SFs) for each library by DESeq2. When comparing libraries normalized by these SF, we considered only enhancers with average normalized read counts $\geq$ 50. *P* values were calculated by the Wald test and false discovery rates (FDRs) by the Benjamini-Hochberg method[16]. Enhancers with normalized read count > 2-fold and FDR < 0.01 were considered enriched in the given subtype. Since the cohort contained several neural-like and HNF+ LNETs but only two tumors

in cluster 3, neural-like were compared against HNF+ LNETs, and both cluster 3 samples against all the rest. Motif analysis was conducted using HOMER's findMotifsGenome with parameters "-size given -mask -bits". To pick the top 3 motif families (Fig. 1) we picked the top 3 motifs, skipping any motif similar to a motif that was already picked.

H3K27ac data of pancreatic and ileal neuroendocrine tumors were taken from ref. [3] and reprocessed as above. Binding sites of HNF1A and HNF4A in HepG2 cells were downloaded from ENCODE, accession ENCFF767MSS and ENCFF263RCV. To generate enhancer heatmap and correlations, HOMER's annotatePeaks function was used, at 5kb window around all peaks except promoter peaks. Tumors were clustered by hierarchical clustering of the Spearman correlations of enhancer acetylation, by shortest distance linkage. Enhancers were clustered by k-means clustering, picking clustering with minimal error of 100 iterations.

RNA-seq reads were mapped to the hg38 reference genome using STAR 2.7.10a (Ref. [17]) and Ensembl release 99 annotations. Reads were counted with featureCounts, discarding reads with mapping quality < 10. Density signals were calculated by deeptools's bamCoverage[11] with BPM normalization. Gene set enrichment analysis was calculated by Fisher exact test using HOMER's findGO script compared to the MSigDB database[18]. Gene set enrichment of differential enhancers was done by associating each enhancer to the nearest TSS, if the distance was < 100kbp, and compared against the list of genes near all enhancers (associating genes similarly), using the -bg parameter of findGO. Relative enrichment score was calculated by: (number of target genes in term * total number of genes)/(total number of target genes * number of genes in term), as suggested in Ref. [19].

Acknowledgments

The present study has been supported by the Neuroendocrine Tumor Research Foundation (YD), and by the Alon Fellowship of the Israeli Council for Higher Education (YD). We thank Prof. Yinon Ben-Neriah (HUJI) for providing us with the A51 inhibitor and helpful discussions.

References

1. Zhou, V. W., Goren, A. & Bernstein, B. E. Charting histone modifications and the functional organization of mammalian genomes. *Nat. Rev. Genet.* **12**, 7–18 (2011).
2. Drier, Y. *et al.* An oncogenic MYB feedback loop drives alternate cell fates in adenoid cystic carcinoma. *Nat. Genet.* **48**, 265–272 (2016).
3. Cejas, P. *et al.* Enhancer signatures stratify and predict outcomes of non-functional pancreatic neuroendocrine tumors. *Nat. Med.* **25**, 1260–1265 (2019).
4. Chapuy, B. *et al.* Discovery and characterization of super-enhancer-associated dependencies in diffuse large B cell lymphoma. *Cancer Cell* **24**, 777–790 (2013).
5. Alcala, N. *et al.* Integrative and comparative genomic analyses identify clinically relevant pulmonary carcinoid groups and unveil the supra-carcinoids. *Nat. Commun.* **10**, 3407 (2019).
6. Laddha, S. V. *et al.* Integrative Genomic Characterization Identifies Molecular Subtypes of Lung Carcinoids. *Cancer Res.* **79**, 4339–4347 (2019).
7. Capdevila, J. *et al.* Lenvatinib in Patients With Advanced Grade 1/2 Pancreatic and Gastrointestinal Neuroendocrine Tumors: Results of the Phase II TALENT Trial (GETNE1509). *J. Clin. Oncol. Off. J. Am. Soc. Clin. Oncol.* **39**, 2304–2312 (2021).
8. Minzel, W. *et al.* Small Molecules Co-targeting CKIα and the Transcriptional Kinases CDK7/9 Control AML in Preclinical Models. *Cell* **175**, 171-185.e25 (2018).
9. Antman, I., Davis, E., Abu-Kamel, S., Hecht, M. & Drier, Y. Simultaneous Mapping of Enhancers and Enhancer Rearrangements with Paired-End H3K27ac ChIP-seq. *Methods Mol. Biol. Clifton NJ* **2535**, 131–140 (2022).
10. Li, H. & Durbin, R. Fast and accurate short read alignment with Burrows-Wheeler transform. *Bioinforma. Oxf. Engl.* **25**, 1754–1760 (2009).
11. Ramírez, F. *et al.* deepTools2: a next generation web server for deep-sequencing data analysis. *Nucleic Acids Res.* **44**, W160–W165 (2016).
12. Heinz, S. *et al.* Simple combinations of lineage-determining transcription factors prime cis-regulatory elements required for macrophage and B cell identities. *Mol. Cell* **38**, 576–589 (2010).
13. Quinlan, A. R. & Hall, I. M. BEDTools: a flexible suite of utilities for comparing genomic features. *Bioinforma. Oxf. Engl.* **26**, 841–842 (2010).
14. Love, M. I., Huber, W. & Anders, S. Moderated estimation of fold change and dispersion for RNA-seq data with DESeq2. *Genome Biol.* **15**, 550 (2014).
15. Liao, Y., Smyth, G. K. & Shi, W. featureCounts: an efficient general purpose program for assigning sequence reads to genomic features. *Bioinformatics* **30**, 923–930 (2014).
16. Benjamini, Y. & Hochberg, Y. Controlling the False Discovery Rate: A Practical and Powerful Approach to Multiple Testing. *J. R. Stat. Soc. Ser. B Methodol.* **57**, 289–300 (1995).
17. Dobin, A. *et al.* STAR: ultrafast universal RNA-seq aligner. *Bioinformatics* **29**, 15–21 (2013).
18. Liberzon, A. *et al.* Molecular signatures database (MSigDB) 3.0. *Bioinformatics* **27**, 1739–1740 (2011).
19. Zeeberg, B. R. *et al.* GoMiner: a resource for biological interpretation of genomic and proteomic data. *Genome Biol.* **4**, R28 (2003).